Dynamics of Bacteria Scanning a Porous Environment

Ehsan Irani,[1] Zahra Mokhtari,[2] and Annette Zippelius[3]
[1]Max Delbrück Center for Molecular Medicine in the Helmholtz Association (MDC), The Berlin Institute for Medical Systems Biology (BIMSB), 10115 Berlin, Germany
[2]Freie Universität Berlin, Department of Mathematics and Computer Science, Institute of Mathematics, Arnimallee 9, 14195 Berlin, Germany
[3]Georg-August-Universität Göttingen, Institut für Theoretische Physik, Friedrich-Hund-Platz 1, 37077 Göttingen, Germany

(Received 1 December 2021; accepted 9 March 2022; published 5 April 2022)

It has recently been reported that bacteria, such as *Escherichia coli* Bhattacharjee and Datta, Nat. Commun. **10**, 2075 (2019). and *Pseudomonas putida* Alirezaeizanjani *et al.*, Sci. Adv. **6**, eaaz6153 (2020)., perform distinct modes of motion when placed in porous media as compared to dilute regions or free space. This has led us to suggest an efficient strategy for active particles in a disordered environment: reorientations are suppressed in locally dilute regions and intensified in locally dense ones. Thereby the local geometry determines the optimal path of the active agent and substantially accelerates the dynamics for up to 2 orders of magnitude. We observe a nonmonotonic behavior of the diffusion coefficient in dependence on the tumbling rate and identify a localization transition, either by increasing the density of obstacles or by decreasing the reorientation rate.

DOI: 10.1103/PhysRevLett.128.144501

The natural habitat of a wide range of micro-organisms are complex crowded media. Examples are micro-organisms that populate and colonize rocks, modeled as microporous spaces, as well as bacteria that contaminate or purify soil [1,2]. In living matter, micro-organisms find themselves in a crowded environment, such as bacteria invading mucus [3–6] or cells invading tissue [7]. In many of these instances, it is vital for the micro-organism to move efficiently through the porous and tortuous environment that they are stuck in. The search for nutrients as well as the escape from a poisonous environment has to be sufficiently fast. Many technical applications, such as water purification and decomposition of contaminants trapped in the ground [8,9] rely on efficient dynamics of bacteria. In medical applications, bacteria are engineered to sense the porous environment of a tumor [10,11] or micro-organisms are designed for drug delivery [12]—fast and efficient dynamics of the bacteria being essential for their task. Despite these widespread applications, there is yet no consensus on how the dynamics of such organisms are adapted to perform most efficiently in a complex and crowded medium. This has led us to ask: What is the best strategy for active agents to explore large porous regions in short time? To what extent can adaptation to the inhomogeneous environment accelerate the dynamics?

Several theoretical studies and simulations have addressed active particles in a random environment [13–18]. Frequently the porous medium is modeled by the Lorentz model [19,20], where static obstacles are placed randomly in space, covering a volume (area) fraction ϕ_o. Zeitz *et al.* [14] simulated active Brownian particles, whose diffusion constant is depressed due to the tendency of active particles to get stuck around obstacles. Reichhardt and Reichhardt [15] include a drift term; surprisingly, the drift velocity is nonmonotonic as a function of run time for given ϕ_o. Bertrand *et al.* [16] compute the diffusion constant of active particles in a lattice gas model and show that the diffusion constant is nonmonotonic in the tumbling rate as long as the obstacles are static (or very slow). More recently, Kurzthaler *et al.* [17] derived a geometric criterion for optimal spreading, when the run length of the bacteria is comparable to the longest straight path in the porous medium. In contrast to these approaches, we suggest a *local* adaptation mechanism of the dynamics. Sensing the local density allows the micro-organisms to adjust their hopping rate efficiently in a strongly inhomogeneous environment. Reorientation in dilute regions is ineffective and hence suppressed; reorientation in dense regions and, in particular, in traps is essential and hence fostered.

Local sensing of the environment has been adopted as a survival mechanism in many phyla throughout the animal kingdom. Several micro-organisms regulate their behavior according to the density of neighbors or to local gradients in phoretic propulsion. For example, a mechanism known as quorum sensing allows bacteria to change their speed according to the density of neighbors [21–28]. Schools of fish have been observed to regulate their speed according to the density of neighbors [29,30]. Regarding chemotaxis of bacteria in porous media, it has been suggested that the tumbling rate [31] as well as the tumbling angle [32] changes in response to the local chemotactic concentration. Bacteria with several swimming modes, such as

Pseudomonas putida [33], can switch between different run modes in response to chemotactic conditions, optimizing their chemotactic strategy. Volpe and Volpe [34] argue that the topography of the environment globally enhances the random motion as compared to the ballistic one. Recent experiments by Bhattacharjee and Datta [35] on bacterial hopping in porous media revealed that random disorder does not just change the tumbling frequency and, consequently, also the run length. Instead, the bacteria are able to change their dynamics if trapped, so that hopping becomes dependent on the geometry of the pore space.

Model.—We consider the dynamics of an elongated tracer particle in a two-dimensional medium of static obstacles with area fraction ϕ_o. The tracer is modeled as a rigid trimer, consisting of three beads of radius R_t. The position vector of the central bead is denoted by $\boldsymbol{r}$. The two peripheral beads are rigidly attached to the central bead, forming a linear configuration, whose orientation is specified by a unit vector $\boldsymbol{n} = (\cos\varphi, \sin\varphi)$. The position vectors of the two peripheral beads are thus given by $\boldsymbol{r}^{\pm} = \boldsymbol{r} \pm 2R_t\boldsymbol{n}$. The trimer is considered a model for an elongated particle of aspect ratio 3. The obstacles are modeled as disks (2D), much larger than the beads of the trimer. In the following, we choose for the ratio of obstacle radius to tracer radius $R_o/R_t = 10$. The interaction of the beads with the obstacles $\boldsymbol{F}(\boldsymbol{r})$ is taken as a contact potential, modeled by a stiff spring.

Since the trimer is modeled as a rigid body, its dynamics is fully characterized by an equation for the translational motion of the center of mass, which is taken to coincide with $\boldsymbol{r}$, and an equation of motion for the orientation φ. We assume overdamped dynamics, according to

$$\dot{\boldsymbol{r}} = \boldsymbol{v}_a + \frac{1}{\gamma}\sum_{i=1}^{N_o}\boldsymbol{F}_i. \tag{1}$$

The total force on the center of mass due to obstacle i at position vector $\boldsymbol{R}_i$, is given by $\boldsymbol{F}_i = \boldsymbol{F}(\boldsymbol{r}-\boldsymbol{R}_i) + \boldsymbol{F}(\boldsymbol{r}^+-\boldsymbol{R}_i) + \boldsymbol{F}(\boldsymbol{r}^--\boldsymbol{R}_i)$. The active velocity $\boldsymbol{v}_a$ is applied along the direction of the trimer $\boldsymbol{n}$. Interactions with the obstacles cause the trimer to rotate,

$$\dot{\varphi} = \sum_{i=1}^{N_o}\tau_i, \tag{2}$$

where the torque $\boldsymbol{\tau}_i$ is explicitly given by $\boldsymbol{\tau}_i = (\boldsymbol{r}^+-\boldsymbol{r})\times\boldsymbol{F}(\boldsymbol{r}^+-\boldsymbol{R}_i) + (\boldsymbol{r}^--\boldsymbol{r})\times\boldsymbol{F}(\boldsymbol{r}^--\boldsymbol{R}_i)$. The torque is always normal to the plane of motion and τ_i is the projection of the vectorial torque on the normal of the plane of motion.

The occasional tumbling of bacteria has been modeled as a stochastic reorientation process. For example, the bacteria reorient in random directions with a given probability. Such a model is widely accepted for run and tumble dynamics in solution. Does it apply also in dense porous media?

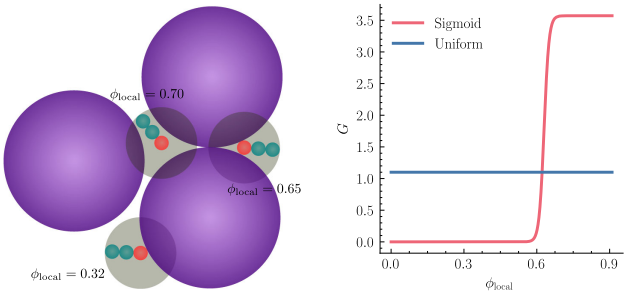

FIG. 1. Left: a hypothetical disk (shown in gray) is defined for each trimer by a concentric area of radius r_l centered around the trimer's head. The local area fraction ϕ_{local} is the overlap of the hypothetical disk with neighboring obstacles. Right: uniform (blue) and sigmoidal (red) G.

Recently, it has been shown [35] that bacterial dynamics are changed when they are trapped. This has led us to introduce a reorientation mechanism that depends on the local environment of the tracer. In particular, the reorientations that disturb the ballistic motion in void space and simultaneously prevent the particles from getting trapped are adapted to the local density in a strongly heterogeneous environment. In that way, we try to model the experimental finding that "hops are guided by the geometry of the pore space" [35].

Physical interactions between bacteria and surfaces are known to be determined by near-field lubrication forces [36–38] and steric collisions [39]. Bacterial responses to such interactions vary from trapping in almost deterministic circular trajectories [37] to enhanced reorientations [40] depending on the type of surface and species. It has also been shown [41–43] that mechanical load on the flagella alters the flagellar motor kinematics and thereby modulates reorientations.

With a rate of $\lambda = 1/t_{\text{re}}$ the local volume fraction ϕ_{local} is calculated inside a region with radius r_l, surrounding the trimer's head (see Fig. 1). We use a function $G(\phi_{\text{local}})$ to generate the probability of performing a random reorientation in the full range from 0 to 2π. The functional form of $G(\phi_{\text{local}})$ incorporates the sensing mechanism that we refer to as "density sensing" in the following. Constant G results in the standard run and tumble dynamics with the rate of $\lambda = 1/t_{\text{re}}$, independent of the local environment. For a more sensitive function to ϕ_{local} we consider a sigmoidal form as

$$G(\phi_{\text{local}}) = \frac{C}{1+\exp^{-k(\phi_{\text{local}}-\phi_0)}} \tag{3}$$

for the reorientation probability, with C being the normalization factor. This choice reflects a high probability of reorientation in a locally dense region and a very low probability in a locally more dilute region. To approximate a step function, we choose $k = 100$ and $\phi_0 = 0.63$.

We want to analyze the dynamics of the tracer particle as a function of several parameters. Without density-dependent reorientation, these are the magnitude of the active velocity v_a and the packing fraction of the obstacles ϕ_o. Including density-dependent reorientation, the important parameter is the timescale t_{re} of reorientation. The size of the region r_l to determine the local density should be comparable to the size of the obstacle. Other functions $G(\phi_o)$, mapping ϕ_{local} to the probability of reorientation, may be considered in future work.

The parameters can be expressed in timescales. We measure lengths in units of $2R_t$ and times in units of the active timescale $t_a = 2R_t/v_a$, which is controlled by the active velocity. In these units, the reorientation time $\tau_{\mathrm{re}} = t_{\mathrm{re}}/t_a$ is the Péclet number. The collision time is given as $t_{\mathrm{coll}}^{-1} = 2v_a R_o N_o/L^2$ or in dimensionless units $t_a/t_{\mathrm{coll}} = 2R_o R_t N_o/L^2$. It is controlled by the area fraction $\phi_o = N_o \pi R_o^2/L^2$. Both tumbling as well as collisions randomize the velocity of the active particle and give rise to diffusion and hence cause a crossover from ballistic to diffusive motion.

We used HOOMD-BLUE [44] to integrate Eq. (1) and run molecular dynamics simulations on a graphics processing unit ($\Delta t_{\mathrm{MD}} = 10^{-2}$). The FREUD package [45] is used to investigate the local environment. For each set of (τ_{re}, ϕ_o), 10–50 simulations are performed, each with 100 independent trimers and $N_o = 2500$ random obstacles without overlaps.

Results.—We focus here on the dynamics of tracer particles adapted to their local environment. In Fig. 2 we show the mean square displacement (MSD) for $G(\phi_{\mathrm{local}})$ (full line) in comparison to a constant G (dashed line). The most striking observation is the strong boost of the dynamics for density sensing, when the reorientation time is comparable to the timescale of active motion. The acceleration is due to uninterrupted ballistic motion as well as reduced trapping times. For moderate densities, such as $\phi_o = 0.4$ shown in Fig. 2, the first mechanism dominates, whereas for rather dense systems, such as $\phi_o = 0.7$, the latter dominates (see below).

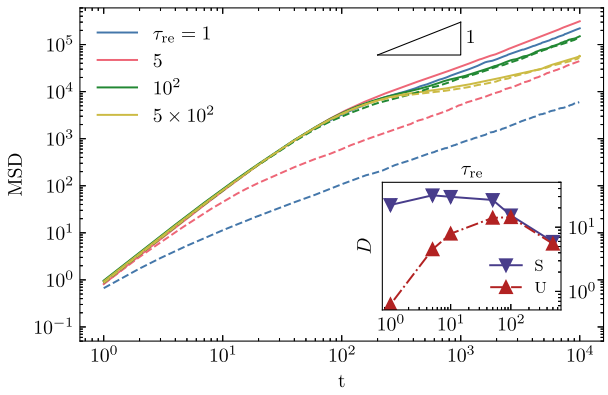

FIG. 2. MSD of trimers for $\phi_o = 0.4$ and different reorientation times τ_{re}. Comparison of sigmoidal (full line) and constant G (dashed line). Inset: diffusion coefficient versus τ_{re}; a sigmoidal function G (blue) is compared to a constant G (red).

To quantify the acceleration due to density sensing, we extract a diffusion constant as the slope of the MSD in the diffusive regime. It is plotted in the inset of Fig. 2 as a function of τ_{re} for both uniform and sigmoidal G. The diffusion constant is larger by almost 2 orders of magnitude for density sensing and $\tau_{\mathrm{re}} \sim 1$, i.e., when the reorientation time is comparable to the timescale of active motion. Furthermore, the diffusion constant is nonmonotonic in τ_{re}, as already observed in Fig. 2. The fastest dynamics is found for $\tau_{\mathrm{re}} \sim 5$ and slows down for increasing as well as decreasing τ_{re}. This nonmonotonic behavior has been observed previously for constant reorientation rate [16], where it is in fact more pronounced. It can be explained by the following intuitive argument: For large τ_{re} the particles are stuck for a long time in a locally dense region of obstacles, so that the diffusion constant is small and approximately inversely proportional to τ_{re}. For small τ_{re}, randomization of the active motion is fast, so that the crossover from ballistic motion to diffusive behavior happens at early times, resulting in small values of the diffusion constant for small τ_{re}. These two effects together give rise to an optimal value for τ_{re}, for which the dynamics is fastest.

The difference between uniform and sigmoidal G disappears for very long reorientation times, when reorientation is so rare that ballistic motion is mainly interrupted by collision events that are the same for both models. It has been suggested recently [17] that reversing the velocity of the active particle is an efficient means to accelerate the dynamics. For the sigmoidal G, random reorientation and run-reverse dynamics can hardly be distinguished (see Fig. 1 in the Supplemental Material).

The boost of the dynamics with density sensing can be traced back to the distribution of waiting times, defined as the time interval between two reorientation events. The distribution is a simple exponential for a uniform G and all densities, characterized uniquely by τ_{re}. In contrast, sigmoidal G gives rise to a second exponential, which slows down dramatically as the density decreases, see Fig. 3(a). In fact, the decay rate β of the distribution increases approximately exponentially with ϕ_o. The long relaxation times for moderate ϕ_o are directly related to increasingly long straight paths for dilute systems. Following Refs. [17,46] we compute the distribution of straight paths that lie entirely in the void space of the porous medium. The distribution of these so-called chord lengths is shown in Fig. 3(b). The distribution strongly resembles the distribution of waiting times. The average waiting time $\langle \tau_{\mathrm{re}}^w \rangle$ is the average distance the trimer travels from one trap to another, divided by the swimming speed. We estimate this distance as the mean chord length [extracted from Fig. 3(b)] times the average number of collisions (evaluated by tracking

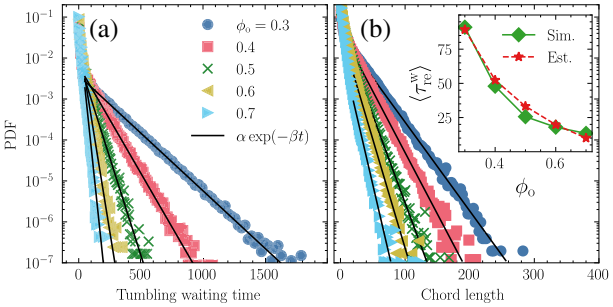

FIG. 3. (a) Probability density function (PDF) of waiting times between two reorientation events. (b) PDF of chord lengths. Inset: mean waiting time from the distribution in the left (Sim.) compared to estimate from chord lengths (Est.). All for different ϕ_o, a sigmoidal G, and $\tau_{re} = 5$.

trajectories) between two tumbling events. The inset of Fig. 3(b) compares this estimate for $\langle \tau_{re}^w \rangle$ to the values computed from the distribution of waiting times [Fig. 3(a)]. The good agreement gives further support to our conclusion that the frequency of reorientation is determined by the geometry of the environment. The latter determines the optimal path for the active particle [47], which is clearly seen in the videos in the Supplemental Material [48]. Interestingly, the mean waiting time $\langle \tau_{re}^w \rangle$ for optimal transport in our model ($\tau_{re} \sim 5$) lies in a similar range as the experimental data [35] suggest (for details, see the Supplemental Material [48]).

The dependence of the dynamics on the area fraction of obstacles is shown explicitly in Fig. 4. As one expects, we see ballistic motion for short times and then a crossover to diffusion at long times. As the density of obstacles ϕ_o is increased, the diffusion constant is reduced and, eventually, at $\phi_o = 0.7$ all particles are localized, exhibiting a plateau in the MSD. The size of the plateau is the average squared localization length and independent of the dynamics. At the localization transition, we observe subdiffusive behavior. The localization transition in the Lorentz model with nonoverlapping obstacles is a percolation transition.

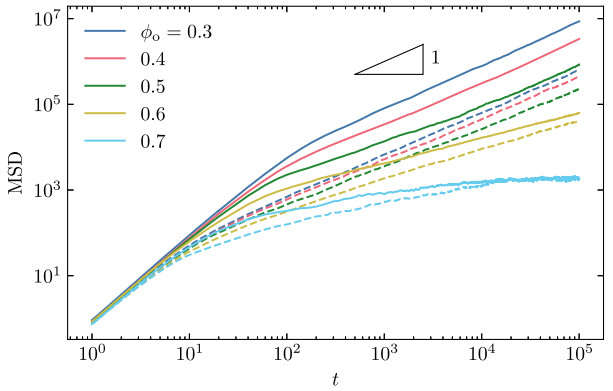

FIG. 4. MSD of trimers for $\tau_{re} = 5$ and different area fraction ϕ_o; comparison of sigmoidal (full line) and constant G (dashed line).

The critical packing fraction for localization ϕ_{crit} depends on the size ratio R_o/R_t and has been computed in [49].

A finite fraction of particles is localized even for $\phi_o < \phi_{crit}$ due to the existence of finite size void regions, coexisting with the macroscopic void area. In fact, the size of these cages is widely distributed; for $\phi_o = 0.4$ it varies over more than 2 orders of magnitude (see Fig. 3 in the Supplemental Material [48] for an example). A quantitative measure of partial localization is provided by $Q(t; d)$, the fraction of particles which have moved less than d in time t. Choosing $d = 0.3L$, we observe that $Q(t; d)$ decays to a finite value even well below $\phi_o = 0.7$, implying that a finite fraction of the particles is localized [see Fig. 5(a)]. As the percolation transition is approached, the relaxation time of $Q(t; d)$ diverges as can be seen in Fig. 5(b), where we plot τ_Q, defined as $Q(\tau_Q; d) = 0.6$. The fraction of localized particles $Q_\infty(d)$ for $\phi_o \leq 0.7$ depends, of course, on the chosen value of d. In Fig. 5, this was chosen comparable to system size in order to show that a finite fraction of particles is localized on scales comparable to system size.

For dense systems, e.g., $\phi = 0.6$, the dominant mechanism responsible for the speedup of transport is the enhanced escape from cages. Whereas, for uniform G, particles reorient as close to the inner boundaries and dead ends of the cage as they do in the center of the cage, for sigmoidal G they effectively reorient only at dead ends, resulting in a negligible number of reorientations, unless it is necessary to escape a trap. Thereby, the mean trapping time is reduced by a factor of approximately 2 for sigmoidal G as compared to uniform G and most pronounced for the highest densities [see Fig. 5(c)].

Localization can also occur for smaller ϕ_o, such as $\phi_o = 0.4$, if the reorientation time is increased accordingly. This is apparent in Fig. 2, where we observe the emergence of a plateau for $\phi_o = 0.4$ and $\tau_{re} \geq 500$. Reorientations are a rare event, but will take place for sufficiently long times.

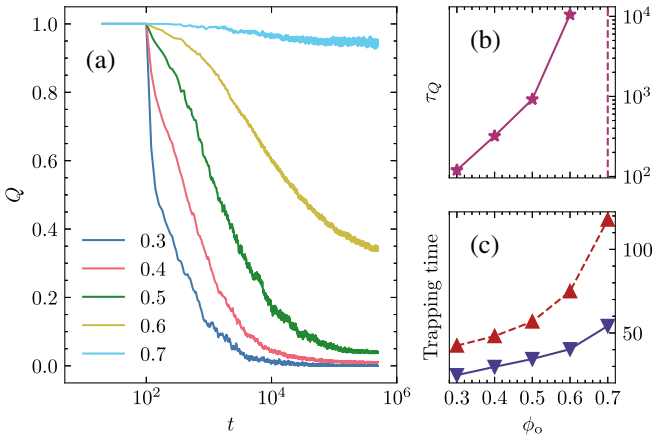

FIG. 5. (a) $Q(t; d)$ for $d = 100$, $\tau_{re} = 5$, and several values of ϕ_o (color coding as in Fig. 4). (b) The relaxation time τ_Q, defined by $Q(\tau_Q; d) = 0.6$, versus ϕ_o. (c) Comparison of mean trapping time for uniform (red) and sigmoidal (blue) G as a function of ϕ_o.

Hence we expect to see a crossover to diffusive behavior for even longer times, in contrast to tracers above the percolation threshold (light blue curve in Fig. 4), which are truly localized. Increasing τ_{re} thus provides another route to glassy dynamics in active matter (see Fig. 1 in the Supplemental Material [48]).

We have introduced a model for bacterial spread in a porous medium, which substantially accelerates the dynamics. It is based on a sensing mechanism of the local density and thereby reduces adverse tumbling in locally dilute regions and enhances necessary reorientations, when the bacteria are trapped in local cages. The extremely long waiting times between successive tumbling events for moderate densities can be traced to the geometry of the porous structure that determines the optimal path of the active agent. For the fully random structure under consideration, the diffusion constant can be enhanced by 2 orders of magnitude. We expect the effect to be even stronger in a structured system whose inhomogeneities extend over finite length scales.

The model can be easily extended to other transport phenomena that require scanning of the environment. A prominent example is chemotaxis, requiring local sensing of food or poison. Here a concentration-dependent tumbling rate may be the simplest model to account for directed motion in a concentration gradient.

E. I thanks support from the Pombo group at Max Delbrück Center for Molecular Medicine in the Helmholtz Association (Germany). Z. M acknowledges Germany's Excellence Strategy—MATH+: The Berlin Mathematics Research Center (EXC-2046/1)—Project ID No. 390685689 (subproject No. EF4-10) for partial support of this project. This work used the computational resources at MDC and the Scientific Compute Cluster at GWDG, the joint data center of Max Planck Society for the Advancement of Science (MPG) and University of Göttingen.

[1] W. Dawid, FEMS Microbiol. Rev. **24**, 403 (2000).
[2] A. J. Wolfe and H. C. Berg, Proc. Natl. Acad. Sci. U.S.A. **86**, 6973 (1989).
[3] S. Cornick, A. Tawiah, and K. Chadee, Tissue Barriers **3**, e982426 (2015).
[4] J. P. Nataro *et al.*, *Colonization of Mucosal Surfaces* (ASM press, 2005), p. 199..
[5] P. S. Cohen and D. C. Laux, in *Methods in Enzymology* (Elsevier, New York, 1995), Vol. 253, pp. 309–314.
[6] J. P. Celli, B. S. Turner, N. H. Afdhal, S. Keates, I. Ghiran, C. P. Kelly, R. H. Ewoldt, G. H. McKinley, P. So, S. Erramilli *et al.*, Proc. Natl. Acad. Sci. U.S.A. **106**, 14321 (2009).
[7] Y. L. Han, A. F. Pegoraro, H. Li, K. Li, Y. Yuan, G. Xu, Z. Gu, J. Sun, Y. Hao, S. K. Gupta *et al.*, Nat. Phys. **16**, 101 (2020).
[8] T. R. Ginn, B. D. Wood, K. E. Nelson, T. D. Scheibe, E. M. Murphy, and T. P. Clement, Adv. Water Resour. **25**, 1017 (2002).
[9] F.-G. Simon, T. Meggyes, and T. Tünnermeier, *Advanced Groundwater Remediation: Active and Passive Technologies* (Thomas Telford Publishing, London, 2002), p. 3.
[10] J. C. Anderson, E. J. Clarke, A. P. Arkin, and C. A. Voigt, J. Mol. Biol. **355**, 619 (2006).
[11] O. Felfoul, M. Mohammadi, S. Taherkhani, D. De Lanauze, Y. Z. Xu, D. Loghin, S. Essa, S. Jancik, D. Houle, M. Lafleur *et al.*, Nat. Nanotechnol. **11**, 941 (2016).
[12] M. Luo, Y. Feng, T. Wang, and J. Guan, Adv. Funct. Mater. **28**, 1706100 (2018).
[13] A. Zöttl and J. M. Yeomans, Nat. Phys. **15**, 554 (2019).
[14] M. Zeitz, K. Wolff, and H. Stark, Eur. Phys. J. E **40**, 23 (2017).
[15] C. Reichhardt and C. J. Olson Reichhardt, Phys. Rev. E **90**, 012701 (2014).
[16] T. Bertrand, Y. Zhao, O. Benichou, J. Tailleur, and R. Voituriez, Phys. Rev. Lett. **120**, 198103 (2018).
[17] C. Kurzthaler, S. Mandal, T. Bhattacharjee, H. Löwen, S. S. Datta, and H. A. Stone, Nat. Commun. **12**, 7088 (2021).
[18] Z. Mokhtari and A. Zippelius, Phys. Rev. Lett. **123**, 028001 (2019).
[19] F. Höfling, T. Munk, E. Frey, and T. Franosch, J. Chem. Phys. **128**, 164517 (2008).
[20] T. Bauer, F. Höfling, T. Munk, E. Frey, and T. Franosch, Eur. Phys. J. Spec. Top. **189**, 103 (2010).
[21] C. Liu *et al.*, Science **334**, 238 (2011).
[22] X. Fu, L.-H. Tang, C. Liu, J.-D. Huang, T. Hwa, and P. Lenz, Phys. Rev. Lett. **108**, 198102 (2012).
[23] M. Cates, D. Marenduzzo, I. Pagonabarraga, and J. Tailleur, Proc. Natl. Acad. Sci. U.S.A. **107**, 11715 (2010).
[24] T. Bäuerle, A. Fischer, T. Speck, and C. Bechinger, Nat. Commun. **9**, 3232 (2018).
[25] C. Abaurrea Velasco, M. Abkenar, G. Gompper, and T. Auth, Phys. Rev. E **98**, 022605 (2018).
[26] A. Fischer, F. Schmid, and T. Speck, Phys. Rev. E **101**, 012601 (2020).
[27] M. Rein, N. Heinß, F. Schmid, and T. Speck, Phys. Rev. Lett. **116**, 058102 (2016).
[28] M. B. Miller and B. L. Bassler, Annu. Rev. Microbiol. **55**, 165 (2001).
[29] Y. Katz, K. Tunstrom, C. Ioannou, C. Huepe, and I. Couzin, Proc. Natl. Acad. Sci. U.S.A. **108**, 18720 (2011).
[30] S. Mishra, K. Tunstrom, I. D. Couzin, and C. Huepe, Phys. Rev. E **86**, 011901 (2012).
[31] N. Licata, B. Mohari, C. Fuqua, and S. Setaysehgar, Biophys. J. **110**, 247 (2016).
[32] T. Bhattacharjee, D. B. Amchin, J. A. Ott, F. Kratz, and S. S. Datta, Biophys. J. **120**, 3483 (2021).
[33] Z. Alirezaeizanjani, R. Großmann, V. Pfeifer, M. Hintsche, and C. Beta, Sci. Adv. **6**, eaaz6153 (2020).
[34] G. Volpe and G. Volpe, Proc. Natl. Acad. Sci. U.S.A. **114**, 11350 (2017).
[35] T. Bhattacharjee and S. Datta, Nat. Commun. **10**, 2075 (2019).
[36] A. P. Berke, L. Turner, H. C. Berg, and E. Lauga, Phys. Rev. Lett. **101**, 038102 (2008).

[37] D. Takagi, J. Palacci, A. B. Braunschweig, M. J. Shelley, and J. Zhang, Soft Matter **10**, 1784 (2014).
[38] O. Sipos, K. Nagy, R. Di Leonardo, and P. Galajda, Phys. Rev. Lett. **114**, 258104 (2015).
[39] K. Drescher, J. Dunkel, L. H. Cisneros, S. Ganguly, and R. E. Goldstein, Proc. Natl. Acad. Sci. U.S.A. **108**, 10940 (2011).
[40] M. Molaei and J. Sheng, Sci. Rep. **6**, 35290 (2016).
[41] K. A. Fahrner, W. S. Ryu, and H. C. Berg, Nature (London) **423**, 938 (2003).
[42] M. J. Tipping, N. J. Delalez, R. Lim, R. M. Berry, and J. P. Armitage, mBio **4**, e00551 (2013).
[43] N. Wadhwa, R. Phillips, and H. C. Berg, Proc. Natl. Acad. Sci. U.S.A. **116**, 11764 (2019).
[44] J. A. Anderson, J. Glaser, and S. C. Glotzer, Comput. Mater. Sci. **173**, 109363 (2020).
[45] V. Ramasubramani, B. D. Dice, E. S. Harper, M. P. Spellings, J. A. Anderson, and S. C. Glotzer, Comput. Phys. Commun. **254**, 107275 (2020).
[46] S. Torquato and B. Lu, Phys. Rev. E **47**, 2950 (1993).
[47] A. Stukowski, Model. Simul. Mater. Sci. Eng. **18**, 015012 (2010).
[48] See Supplemental Material at http://link.aps.org/supplemental/10.1103/PhysRevLett.128.144501 for videos and extra plots regarding the trimer's displacements and glassy dynamics.
[49] S. K. Schnyder, M. Spanner, F. Höfling, T. Franosch, and J. Horbach, Soft Matter **11**, 701 (2015).